Electronic Supplementary Material (ESI) for Journal of Materials Chemistry A. This journal is © The Royal Society of Chemistry 2017

Hydrogel-Embedded Tight Ultrafiltration Membrane with Superior Anti-Dye-Fouling Property for Low-Pressure Driven Molecule Separation

Gaoshuo Jiang,[a,c] Shenxiang Zhang,[a] Yuzhang Zhu,[a] Shoujian Gao,[a] Huile Jin,[b] Liqiang Luo,[c] Feng Zhang,*[a] Jian Jin*[a]

*Corresponding authors. Email: jjin2009@sinano.ac.cn; fzhang2011@sinano.ac.cn

[a]CAS Key Laboratory of Nano-Bio Interface, i-Lab, and CAS Center for Excellence in Nanoscience, Suzhou Institute of Nano-Tech and Nano-Bionics, Chinese Academy of Sciences, Suzhou, 215123, P. R. China.
[b]College of Chemistry and Materials Engineering, Wenzhou University, Wehzhou, Zhejiang, 325035, China.
[c]Department of Chemistry, Shanghai University, Shanghai 200444, China

Experimental Section

Fabrication of PAAS-m-PAN membranes/coatings: PAN powder (Mw: 150 000, purchased from Sigma-Aldrich) was firstly dissolved in NMP with the concentration of 12% (wt/v, g/mL). Into the NMP solution, different volume of EtOH was added, namely 0%, 5%, 10%, 15%, 20%, 25% and 30% volume percentage of EtOH used in this work, respectively. The NMP/EtOH mixed solution was stirred at 80°C for 12 hours to form a dope solution. The dope solutions (0%, 10% and 20% EtOH, respectively) were casted onto a pre-cleaned glass substrate via a doctor blade and then immersed into a coagulation bath containing 10 wt% NaOH for 40 minutes at 50°C to carry out the alkaline-induced phase inversion and the corresponding PAAS-m-PAN membranes were finally obtained. The PAAS-m-PAN coatings on the cloth fabric and glass fiber sleeving were prepared by scraping the dope solution containing 20% EtOH onto the above pre-cleaned materials via a doctor blade and then immersing them into a coagulation bath containing 10% NaOH for 40 minutes at 50°C. The obtained membranes or coatings were rinsed with deionized water several times and stored in deionized water. As a comparison, PAN membrane prepared from the NMP solution without addition of EtOH was also obtained.

Evaluation of separation performance: The pressure-driven filtration experiment was performed on a dead-end filtration device (Millipore Corp., USA) with an effective area of 2.54 cm^2 under pressure of 1 bar at room temperature. In general, 20 mL of the feed solution containing a certain concentration of solutes was filtered through the membrane. The concentration of the solutes in the feed and permeate solutions were detected by UV-vis absorption spectroscopy. The concentration of the inorganic salts in the feed and permeate solutions were detected by the electrical conductivity. All the data of rejection and water permeance were obtained from the average value of three individual measurements. The water permeance (J_w) was calculated as the following equation:

$$J_w = \frac{V}{S \times t \times P}$$

where V is the volume of the permeate, S is the effective area, t is the operation time, and P is the driving pressure.

The rejection (R) of molecules was calculated according to the following equation:

$$R\ (\%) = \left(1 - \frac{C_p}{C_o}\right) \times 100\%$$

where C_p and C_o are the concentrations of the molecule in the permeate and in the original solution, respectively.

Materials characterization: SEM images were obtained on a field-emission scanning electron microscope (Hitachi S4800, Japan). FTIR spectra were measured on a Nicolet 6700 FTIR spectrometer. Water contact angle measurements were conducted on a Data-Physics OCA 20 at room temperature by employing a 2 μL water droplet. The underwater oil-adhesive force was measured using a high-sensitivity micro-electro-mechanical balance system DLS measurement was done on a Malven Zen 3600. Viscosity measurement was done on a HAAKE RheoStress 6000 (Haake RS6000). UV-vis spectra were measured on a Lambda-25 spectrometer (Perkin-Elmer Inc, USA). The electrical conductivity was measured using a conductometer (FE30K, Mettler Toledo). The concentration of PEG was measured using the Aurora 1030W total organic carbon (TOC) analyzer. Optical microscopy images were taken on a Nikon AZ100 (Japan). The charge property of tight ultrafiltration membrane surface was determined by streaming potential measurement with a SurPASS 3 electrokinetic analyzer (SurPASS, Anton Paar GmbH, Austria). Surface roughness was characterized on an atomic force microscopy(AFM)(Bruker ICON-Dimension) in the tapping mode at room temperature in air.

1. DLS of dope solutions

When no EtOH is added into the dope solution, no peaks are detected by DLS, suggesting no PAN aggregates in the solution (Fig. S1a). When EtOH is added into dope solutions with concentration of 5%, 10%, 15% and 20%, respectively, the solutions still keep clear and transparent but particle peaks are detected by DLS, indicating the formation of polymer aggregates in the solutions. The size of the aggregates slightly increases with increasing the EtOH content (Fig. S1b-S1e). When EtOH content increases to 25% and 30%, the solutions become turbid seriously (Fig. S1f-S1g).

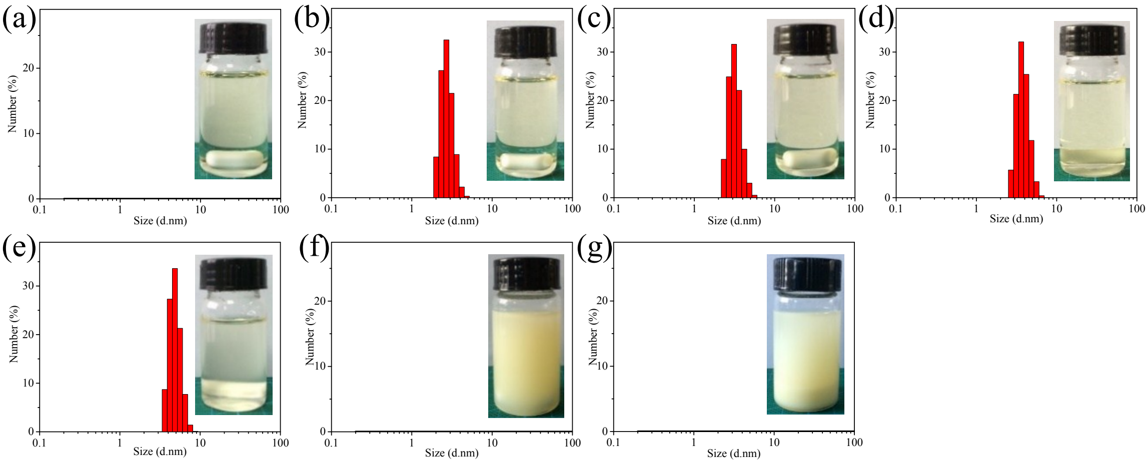

Fig. S1. DLS data of the dope solutions containing different EtOH contents. a) 0%, b) 5%, c) 10%, d) 15%, e) 20%, f) 25%, and g) 30%.

2. Viscosity of dope solutions

The viscosity of the dope solutions containing different content of EtOH is shown in Fig. S2. The viscosity gradually increases with increasing the EtOH content from 0% to 20%. When EtOH content excesses 20%, the viscosity sharply decreases.

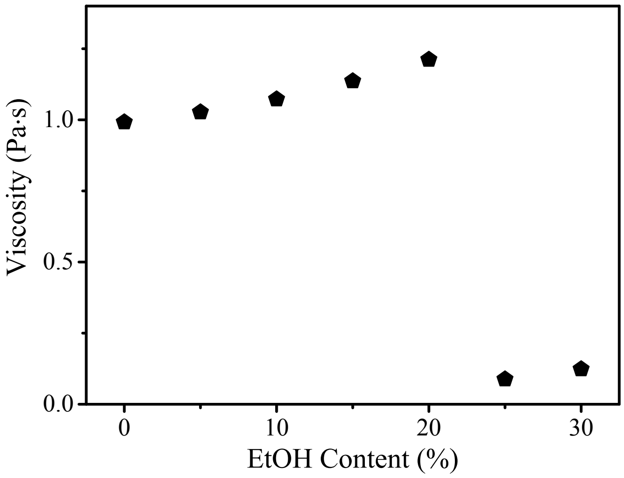

Fig. S2. Viscosity of dope solutions containing different content of EtOH.

3.The effect of the NaOH in the coagulation bath

As for the role of alkaline-assisted phase inversion in memebrane structure, it has been discussed and explained in our previous work.[1] It is considered that the addition of NaOH in coagulation bath inspires the localized micro phase separation of PAN and leads to the membrane with rougher surface. To further clarify the role of NaOH in memebrane structure, the SEM images of the membranes prepared with and without addition of NaOH were characterized as shown in the following figure. It indicates that the existence of NaOH induces a slightly rougher membrane surface than the membrane without NaOH. Besides, when no EtOH was added, the membrane prepared without addition of NaOH exhibits a much larger pores than the membrane prepared with addition of NaOH.

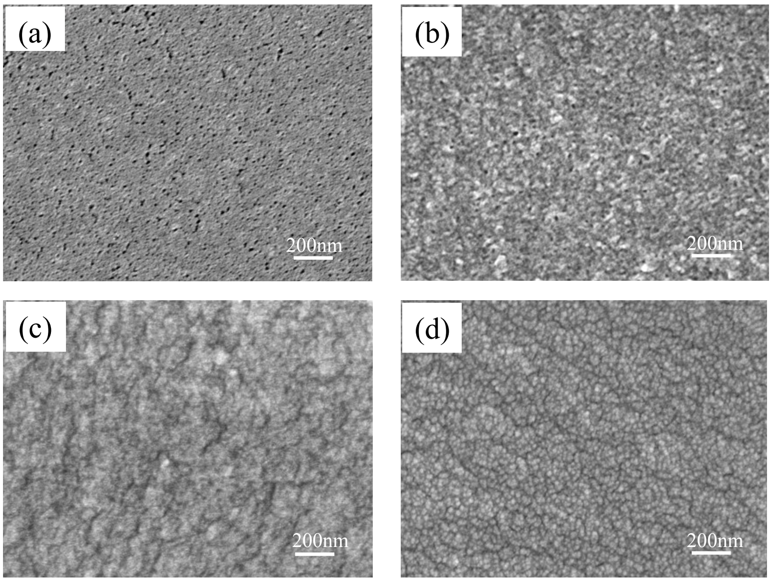

Fig. S3. Top-view SEM image of (a) PAN membrane (0% EtOH, 0% NaOH), (b) PAAS-m-PAN membrane (0% EtOH, 10% NaOH), (c) PAN membrane (20% EtOH 0% NaOH), and (d) PAAS-m-PAN membrane (20% EtOH, 10% NaOH)

4. Cross-section SEM images of the membrane prepared without addition of EtOH

To study the effect of EtOH on the membrane morphology, the PAN membrane prepared from the dope solution without addition of EtOH is characterized as shown in Fig. S4. It shows a typical fingerlike support structure with a dense skin layer on the top surface.

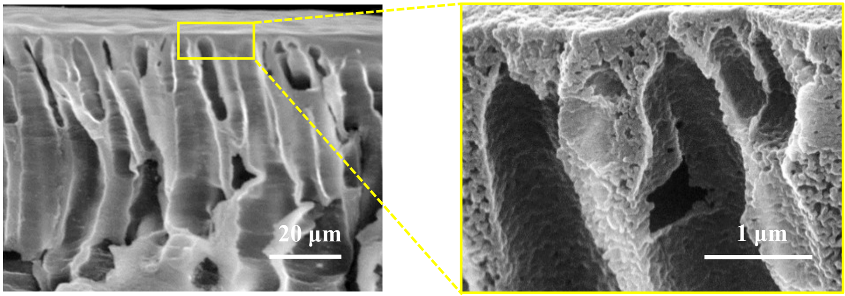

Fig. S4. Cross-section SEM images of the PAN membranes prepared from the dope solution without addition of EtOH.

5. Measurement of hydrolysis degree of PAAS-m-PAN membranes

The titration method is used to determine the degree of hydrolysis of our membranes. Briefly, a membrane is immersed into a 2 M HCl solution for 30 minutes to liberate Na^+ and the membrane is then rinsed by deionized water for ten times at room temperature. After that, the membrane is immersed in a 1 M NaCl solution overnight to liberate H^+ ions. Phenolphthalein is chosen as an indicator to determine the end-point of titration. The H^+-containing solution is then titrated with 0.01 M NaOH. The membrane is kept in the solution during the whole titration process. By recording the volume of the used NaOH solution during the titration process, the concentration of H^+ ions in the solution is obtained and the weight of the hydrolyzed PAN (W_h) is thus acquired. The corresponding hydrolysis degree is finally calculated according to the following Equation.

$$D_h = \frac{W_h}{W_t} \times 100\% \qquad \text{Equation S1}$$

where D_h denotes the degree of hydrolysis, W_h denotes the weight of the hydrolyzed PAN containing sodium acrylate group, W_t denotes the total weight of the membrane.

6. Measurement of water capture percentage

The water capture percentage (*WCP*) is measured by using the equation below:

$$WCP\ (\%) = \frac{W_b - W_a}{W_b} \times 100\% \qquad \text{Equation S2}$$

Where W_b is the mass of the membrane taken out from water and blotted up the surface water. W_a is the mass of the membrane desiccated in drying oven for 6 h.

7. Measurements of the roughness of the membranes

The surface roughness of the membrane was evaluated by AFM characterization as shown in Fig. S5. It shows that the roughness of PAAS-m-PAN membranes is slightly higher than the PAN membrane.

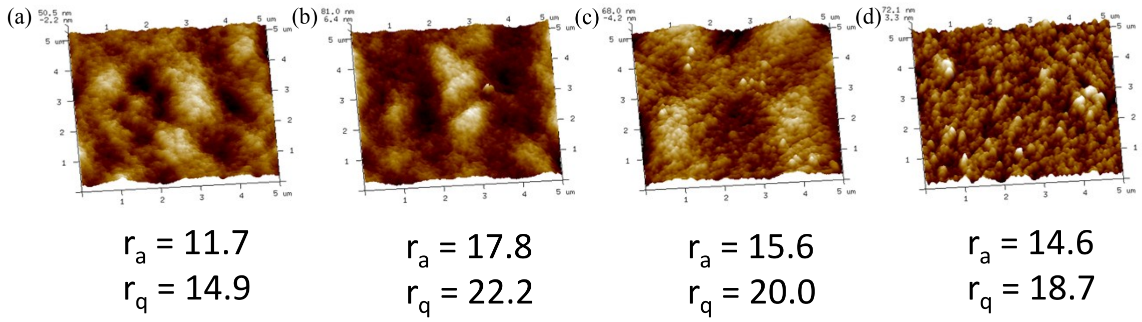

Fig. S5. AFM images of a) PAN membrane and the PAAS-m-PAN membranes prepared from dope solutions containing EtOH of b) 0%, c) 10% and d) 20%, respectively (r_a:mean roughness; r_q : root-mean-square roughness).

8. Measurements of the zeta potential of the membrane surfaces

The samples were measured in a 1 mM KCl background electrolyte solution. The pH of the solution was accommodated using the 0.01 M HCl and 0.01 M NaOH acid-base adjust-pair.

To investigate the influence of surface charge on membrane properties, the zeta potential of the PAAS-m-PAN membranes and the PAN membrane were measured, and the results are shown in Fig. S6. The PAAS-m-PAN membrane surfaces showed similar negative zeta potential values in pH range of 3.1~9.3, while the PAN membrane surface was slightly more negatively charged than the PAAS-m-PAN membrane surfaces.

Compared to the PAAS-m-PAN membrane, the PAN membrane behaves more negatively charged in the pH range of 3.1-9.3. However, the PAN membrane shows very poor anti-dye-fouling property as already shown in Fig. S11a in comparison with PAAS-m-PAN membrane. This result indicates that surface zeta potential play less important role at anti-dye-fouling ability in our work. The anti-dye-fouling property of our membrane is mainly attributed to its strong hydration ability of hydrogel property caused by PAAS.

It shows that the membrane (20%EtOH 10%NaOH)surface is negatively charged in pH range of 3.1 ~ 9.3 and the isoelectric point is at pH $\approx$ 3.1. In table 1, the CBB rejection at pH = 3.1, 6.3, and 9.3 are 96.3 ± 0.3, 98.0 ± 0.3%, and 99.0 ± 0.2%, respectively. It indicates that pH has little effect on the dye rejection. This result reveals that the dye rejection of our membrane is mainly attributed to the molecular sieving effect.

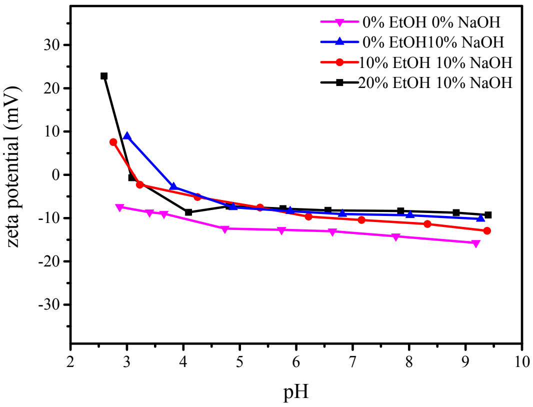

Fig. S6. The zeta potential of the PAN membrane, and the PAAS-m-PAN membranes prepared from dope solutions containing EtOH of 0%, 10% and 20%, respectively.

9. Measurements of rejection and permeance of the membranes to CR

Fig. S7 shows that the membrane prepared from the dope solution without addition of EtOH has the highest water permeance up to 343 Lm^{-2} h^{-1} bar^{-1} but a lowest CR rejection of 74%. With increasing the EtOH content, the permeance decreases while the dye rejection increases correspondingly. As for the PAAS-m-PAN membrane prepared from 20% EtOH content, a CR rejection up to 95% and a permeance of 123 Lm^{-2} h^{-1} bar^{-1} are achieved.

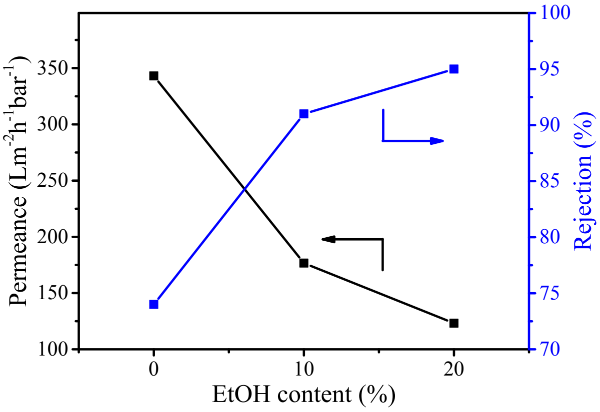

Fig. S7. CR rejection and permeance of the PAAS-m-PAN membranes prepared from dope solutions containing EtOH of 0%, 10% and 20%, respectively.

10. Fitting formula of the effective pore size distribution

The MWCO of the PAAS-m-PAN is defined as the molecular weight of PEG solute at R = 90%. In this work, a log-normal distribution plot is used to obtain the pore size information of the membrane between the rejection and the Stokes radius. The Stokes radius of the PEG solute can be calculated based on its average molecular weight (Equation S3). Through the probability density function (Equation S4), the pore size distribution of the membrane can thus be obtained.

$$r_p = 16.73 \times 10^{-12} \times MW^{0.557} \qquad \text{Equation S3}$$

$$\frac{dR(r_p)}{dr_p} = \frac{1}{r_p ln\sigma_p \sqrt{2\pi}} exp\left[- \frac{(lnr_p - ln\mu_p)^2}{2(ln\sigma_p)^2} \right] \qquad \text{Equation S4}$$

Where r_p is in m and *MW* is in g/mol,μ_p is defined at the PEG rejection of 50% and represents mean effective pore radius and σ_p is determined at the ratio of r_p at R = 84.13% over that at R = 50%.

11. UV–vis absorption spectra of the dye solutions before and after permeation

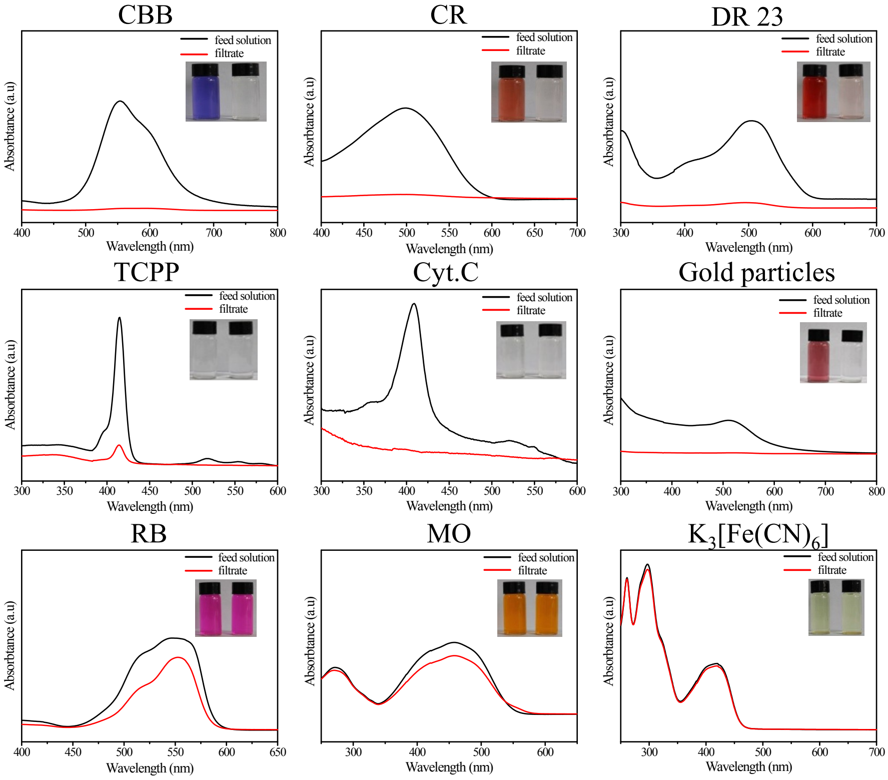

Fig. S8. UV–vis absorption spectra of the feeds and the permeates of 9 different solutions before and after the separation by the PAAS-m-PAN membrane prepared from 20% EtOH dope solution. The insets are the corresponding optical images of the feeds and the permeates.

12. The separation of the solutions containing both dyes and inorganic salts

In order to mimic the actual textile effluent, we prepared the solutions containing both dyes and inorganic salts with different concentrations and permeated them through our membrane. The results were shown in Table S1.

Table S1 | separation performances of the mixed solutions

components	Dye rejection (%)	Salt rejection (%)	Permeance ($Lm^{-2}h^{-1}bar^{-1}$)
100 ppm Congo Red; 5 g/L NaCl	96.5 ± 0.2	1.9 ± 0.2	115 ± 6
100 ppm Congo Red; 10 g/L NaCl	97.2± 0.5	1.8 ± 0.1	108 ± 3
100 ppm Congo Red; 20 g/L NaCl	97.4± 0.3	2.0± 0.2	106 ± 3
100 ppm Congo Red; 40 g/L NaCl	96.7± 0.5	1.9 ± 0.2	99 ± 5

13. The mixed dye separation performance of the membrane

The mixed dye separation performance of the membrane was measured where dye mixture solution containing both CBB (Coomassie brilliant blue) and MO (Methyl orange) with same concentration of 20 mg/L was used as feed solution to permeate the membrane under the driving pressure of 1 bar. The optical image and UV-vis spectra befor and after the separation were shown in Fig. S9. It shows that after one time separation the peak of MO could be observed in the UV-vis absorption spectrum of permeate but no CBB peak is observed. It indicates that the CBB molecules could be completely rejected by the membrane and the MO molecules could pass through the membrane.

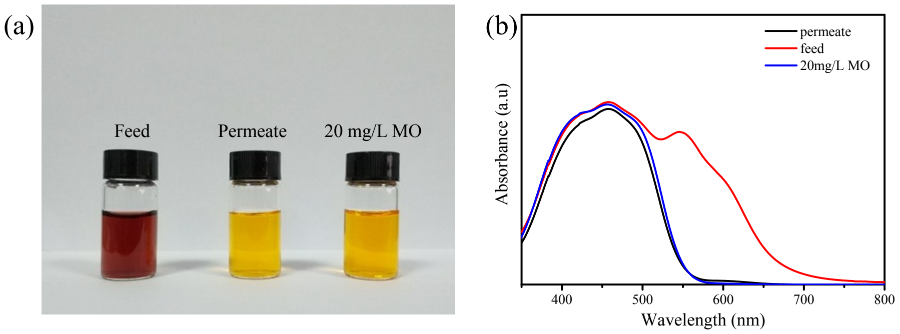

Fig. S9. (a) Optical images and (b) UV-vis absorption spectra of the mixed solution containing CBB and MO with same concentration of 20 mg/L before (feed) and after (permeate) membrane permeation. The pure solution containing 20mg/L MO only is shown in the figures as a reference.

14. Confirmation of molecule sieving effect

To clarify the effect of molecule absorption on the membrane, a method of calculating rejection using the retentate is also adopted in this work where the separation of CBB solution is conducted using a dead-end mode and the feed solution, the retentate and the permeate are all collected. Their UV-vis absorption spectra are presented in Fig. S10a (The volume of retentate is diluted to the same volume as initial feed solution). The collection of the feed, the retentate and the permeate is schematic illustrated in Fig. S10b. The calculation formula is given in Equation S5. It shows that the UV-vis absorption spectroscopy of the feed and the diluted retentate coincides well each other. It indicates that adsorption has almost no effect on the separation performance. The separation is mainly contributed to the molecule sieving effect.

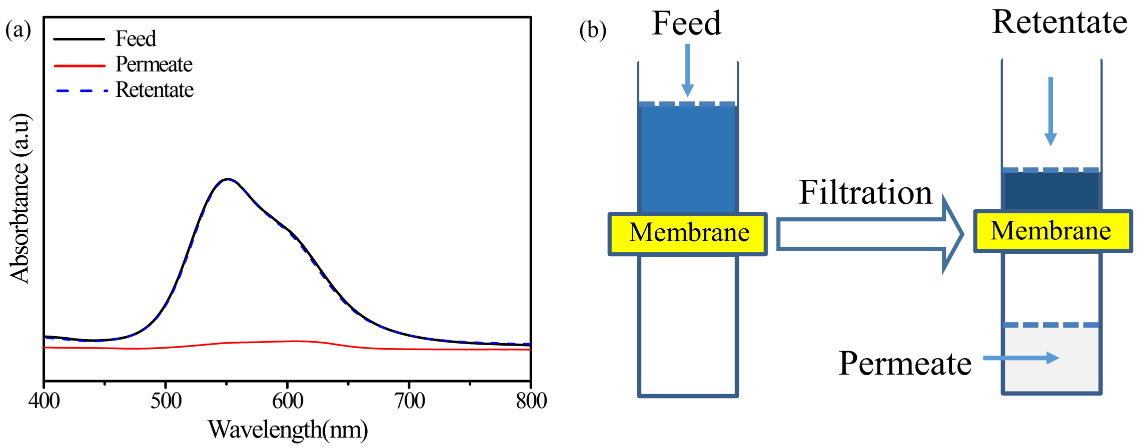

Fig. S10. UV-vis absorption spectroscopy of the feed, permeate and retentate of CBB.

The calculation formula of Fig. S10 is as follows:

$$R = \frac{C_R \times V_R}{C_O \times V_O} \times 100\% \qquad \text{Equation S5}$$

Where C_R is the molecule concentration in retentate, C_O is the molecule concentration in original feed solution (V is their corresponding volume).

15. Anti-dye-fouling test of PAN membrane, PAA-m-PAN membrane and commercial PES membrane.

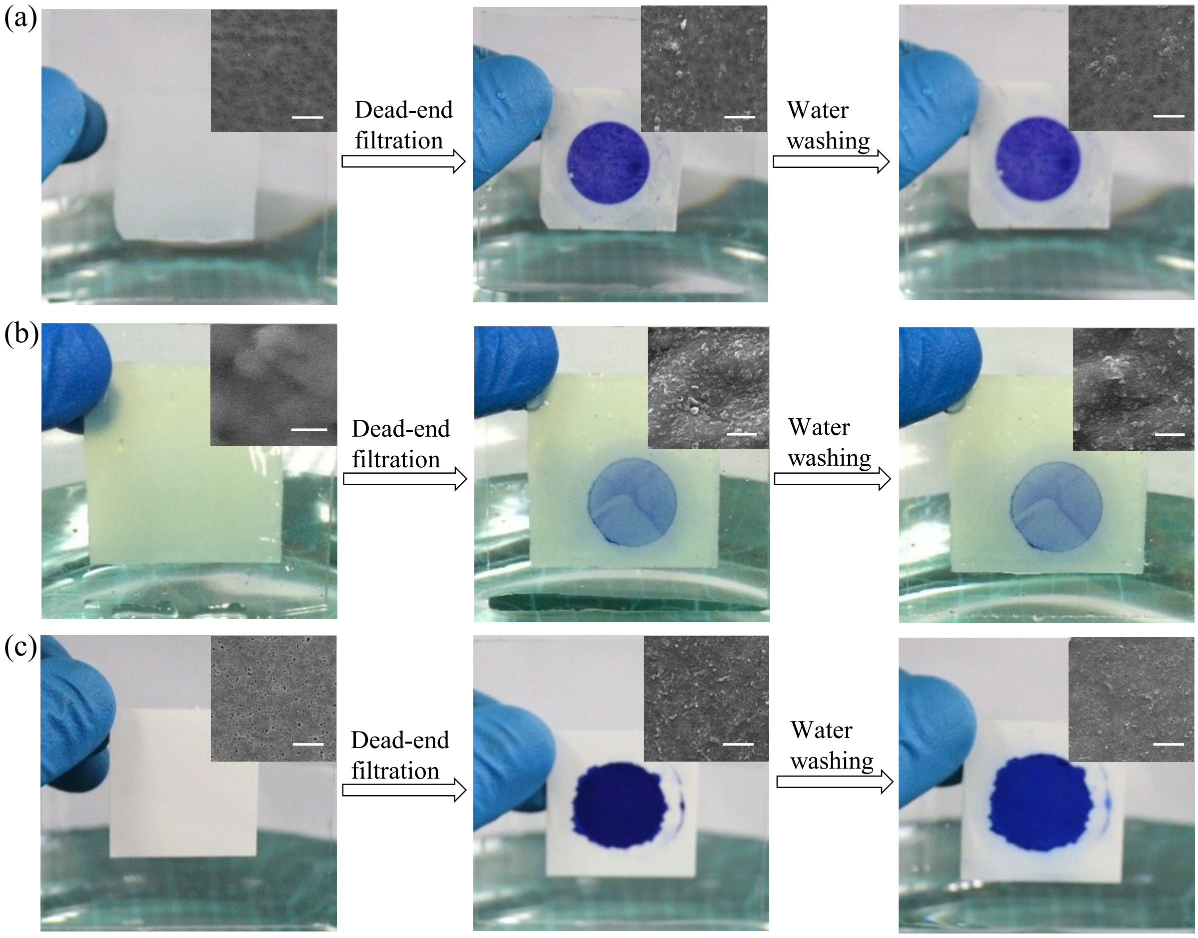

Fig. S11. Optical images and corresponding SEM images of the membranes before and after dye separation. a) PAN membrane fabicated from the dope solution without EtOH addition and coagulation bath without NaOH addition. b) PAAS-m-PAN membrane after immersed in 2 M HCl solution for 30 minutes. During this process, most of sodium acrylate groups transform to acrylic acid groups. c) Commercial PES membrane (purchased from Shenghe Science and Technology Development Center, 0.45 μm). The results show that dyes adsorb seriously on these membranes and can not be removed completely (Scale bar: 5 μm). The anti-dye-fouling property is mainly ascribed to the sodium acrylate groups due to its hydrogel nature.

16. Anti-crude-oil-fouling property of PAAS-m-PAN membrane.

The anti-crude-oil-fouling property of PAAS-m-PAN membrane is also detected as shown in Fig. S12. When forcing a heavy crude oil droplet to fully contact the membrane surface and then withdraw it under water, no adhesion force is detected. The oil could be lifted off the membrane without deformation. What's more, the oil droplet spontaneously releases from the membrane surface once immersed in water.

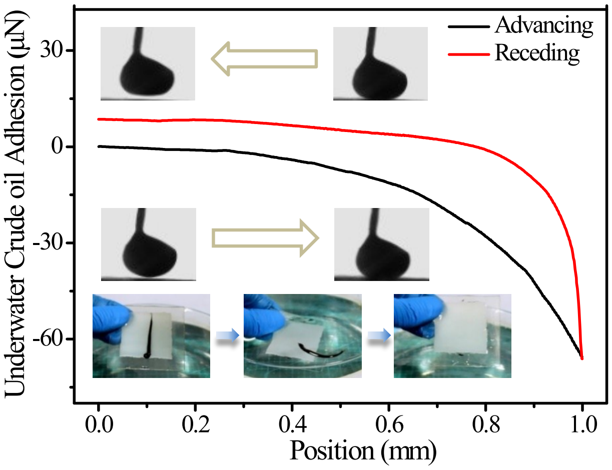

Fig. S12. Real-time recorded force–distance curves during the dynamic oil-adhesion measurement of the PAAS-m-PAN membrane prepared from dope solution conntaining 20% EtOH. A heavy crude oil droplet is used as the detecting probe herein.

17. Stability of PAAS-m-PAN membrane in water.

To confirm the stability of PAAS-m-PAN membrane, the membrane is immersed in water for a long time and its mass and thickness are detected. As shown in Fig. S13, both the mass and thickness of the membrane keep little change during the detected time, indicating the membrane structure is stable in water.

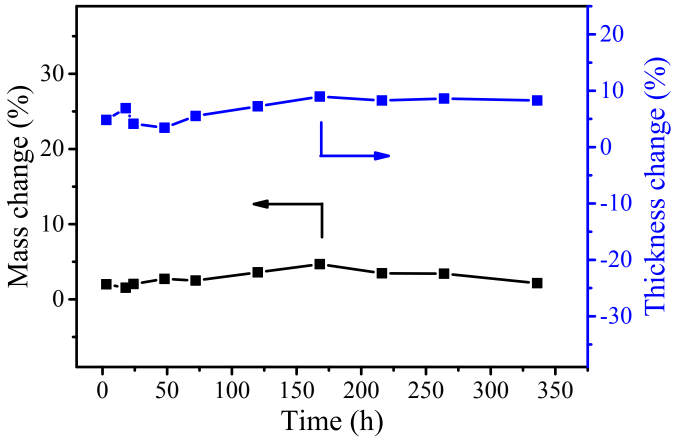

Fig. S13. Variation of mass and thickness of the PAAS-m-PAN membrane as a function of time in water.

18. Mechanical strength of membranes

The mechanical strength of PAN membrane and the PAAS-m-PAN membranes prepared from the dope solutions containing different EtOH contents are examined as shown in Fig. S14. The PAN membrane possesses a highest break strength up to 0.77 MPa and a low engineering strain of 17%. The three PAAS-m-PAN membranes exhibit good engineering strain of 30%, 28% and 22% but with reduced break strength of 0.73 MPa, 0.40 MPa and 0.24 MPa, respectively.

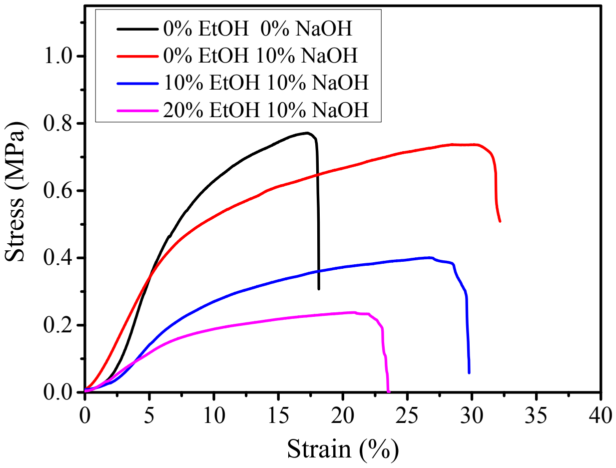

Fig. S14. Stress-strain curves of PAN membrane and the PAAS-m-PAN membranes prepared from the dope solutions containing different EtOH contents.

19. Summary of membrane performance

Table S2 | Summary of the separation performance of previously reported tight UF membranes, tight UF membranes, and ours for dye/salt separation.

Menbrane	Pressure (bar)	Permeance ($Lm^{-2}h^{-1}bar^{-1}$)	Molecule	Rejection (%)	Anti-fouling characterization	reference
Co-NF-2	8	18.2	congo red	99.5	Antimicrobial activity	2
Sepro NF 6	6	13.3	congo red	99.93	No characterization	3
Sepro NF 2A	6	9.585	congo Red	99.96	No characterization	3
HNTs-PIL/PES	6	7.75	reactive black 5	>90	No characterization	4
Sericin–TMC	5	13.5	congo red	99.8	SA and BSA	5
NTR 7450	5	13	reactive blue 2	86.4	No characterization	6
Positively charged loose NF	5	12	methylene blue	99.4	BSA	7
GCNTm	5	11.3	direct yellow	99	BSA, SA and HA	8
Cross-linked PAN/Boltorn	5	10.86	methyl blue	97.6	No characterization	9
PDA/PEI	4	26.2	reactive orange 16	98.1	No characterization	10
PAEK-COOH	4	25.225	congo red	99.8	Protein and dyes	11
SiO2-PSS/ PES	4	23.25	reactive black 5	>90	BSA	12
Zwitterion-hydrotalcite	4	20.05	reactive red 49	86.7	No characterization	13
CS-MMT/PES	4	17.205	reactive red 49	89	BSA	14
GO-PSBMA/PES	4	9.375	reactive red 49	97.2	BSA	15
mHT/PES	4	6.325	reactive black 5	95	No characterization	16
M-PEI	4	3.5	orange II sodium salt	96.8	No characterization	17
PEI/CMCNa/PP	3	17.333	brilliant green	99.8	Dyes	18
CMCNa/PP	3	9.9	congo red	99.8	Dyes	19
PEI crosslinked TUF	2	91.1	congo red	99.9	No characterization	20
ceramic membrane	2	43.5	reactive black 5	98	No characterization	21
UH004	2	27	rirect red 23,	98	No characterization	22
Modified PEI	2	25.5	methyl blue	97.3	BSA, HA and SA	23
TMC composite	2	23.4	orange GII	99.8	HA, SA and BSA	24
TA–Fe^{III}/PES	2	22.8	orange GII	94.8	No characterization	25
GOQD	2	11.65	methyl blue	97.6	BSA	26
Composite NF	1	46.1	congo red	99	BSA, oil and HA	27
Mineralized PAN	1	25.5	congo red	98	No characterization	28
CaAlg	1	16.55	congo red	99.5	BSA	29
ZIF-8	1	5	rose bengal	92.5	No characterization	30
PAAS-m-PAN	1	144	CBB	98.0	Dyes and crude oils	This work
PAAS-m-PAN	1	123	congo Red	95.6	Dyes and crude oils	This work

Supplementary References

1 F. Zhang, S. Gao, Y. Zhu and J. Jin, *J. Membr. Sci.*, 2016, **513**, 67-73.

2 J. Zhu, A. Uliana, J. Wang, S. Yuan, J. Li, M. Tian, K. Simoens, A. Volodin, J. Lin, K. Bernaerts, Y. Zhang and B. Van der Bruggen, *J. Mater. Chem. A*, 2016, **4**, 13211-13222.

3 J. Lin, W. Ye, H. Zeng, H. Yang, J. Shen, S. Darvishmanesh, P. Luis, A. Sotto and B. Van der Bruggen, *J. Membr. Sci.*, 2015, **477**, 183-193.

4 J. Lin, C. Y. Tang, W. Ye, S. P. Sun, S. H. Hamdan, A. Volodin, C. V. Haesendonck, A. Sotto, P. Luis and B. Van der Bruggen, *J. Membr. Sci.*, 2015, **493**, 690-702.

5 C. Zhou, Y. Shi, C. Sun, S. Yu, M. Liu and C. Gao, *J. Membr. Sci.*, 2014, **471**, 381-391.

6 B. V. D. Bruggen, B. Daems, D. Wilms and C. Vandecasteele, *Sep. Purif. Technol.*, 2001, **22-23**, 519-528.

7 F. Liu, B. R. Ma, D. Zhou, L. J. Zhu, Y. Y. Fu and L. X. Xue, *React. Funct. Polym.*, 2015, **86**, 191-198.

8 Y. Han, Y. Jiang and C. Gao, *ACS Appl. Mater. Interfaces*, 2015, **7**, 8147-8155.

9 L. Wang, S. Ji, N. Wang, R. Zhang, G. Zhang and J. R. Li, *J. Membr. Sci.*, 2014, **452**, 143-151.

10 J. Wang, J. Zhu, M. T. Tsehaye, J. Li, G. Dong, S. Yuan, X. Li, Y. Zhang, J. Liu and B. Van der Bruggen, *J. Mater. Chem. A*, 2017, **5**, 14847-14857.

11 L. Xing, N. Guo, Y. Zhang, H. Zhang and J. Liu, *Sep. Purif. Technol.*, 2015, **146**, 50-59.

12 C. Liu, H. Mao, J. Zheng and S. Zhang, *J. Membr. Sci.*, 2017, **530**, 1-10.

13 J. Wang, Y. Zhang, J. Zhu, J. Hou, J. Liu and B. Van der Bruggen, *J. Membr. Sci.*, 2016, **510**, 27-37.

14 J. Zhu, M. Tian, Y. Zhang, H. Zhang and J. Liu, *Chem. Eng. J.*, 2015, **265**, 184-193.

15 J. Zhu, M. Tian, J. Hou, J. Wang, J. Lin, Y. Zhang, J. Liu and B. Van der Bruggen, *J. Mater. Chem. A*, 2016, **4**, 1980-1990.

16 L. Yu, J. Deng, H. Wang, J. Liu and Y. Zhang, *ACS Sustainable Chem. Eng.*, 2016, **4**, 3292-3304.

17 T. Wang, H. Qiblawey, E. Sivaniah and A. Mohammadian, *J. Membr. Sci.*, 2016, **511**, 65-75.

18 Q. Chen, P. Yu, W. Huang, S. Yu, M. Liu and C. Gao, *J. Membr. Sci.*, 2015, **492**, 312-321.

19 S. Yu, Z. Chen, Q. Cheng, Z. Lü, M. Liu and C. Gao, *Sep. Purif. Technol.*, 2012, **88**, 121-129.

20 C. Liu, H. Mao, J. Zheng and S. Zhang, *J. Membr. Sci.*, 2017, **538**, 58-67.

21 X. Ma, P. Chen, M. Zhou, Z. Zhong, F. Zhang and W. Xing, *Eng. Chem. Res.*, 2017, **56**, 7070-7079.

22 J. Lin, W. Ye, M. C. Baltaru, Y. P. Tang, N. J. Bernstein, P. Gao, S. Balta, M. Vlad, A. Volodin, A. Sotto, P. Luis, A. L. Zydney and B. Van der Bruggen, *J. Membr. Sci.*, 2016, **514**, 217-228.

23 S. Zhao and Z. Wang, *J. Membr. Sci.*, 2017, **524**, 214-224.

24 Y. Zhang, Y. Su, J. Peng, X. Zhao, J. Liu, J. Zhao and Z. Jiang, *J. Membr. Sci.*, 2013, **429**, 235-242.

25 L. Fan, Y. Ma, Y. Su, R. Zhang, Y. Liu, Q. Zhang and Z. Jiang, *RSC Adv.*, 2015, **5**, 107777-107784.

26 C. Zhang, K. Wei, W. Zhang, Y. Bai, Y. Sun and J. Gu, *ACS applied materials & interfaces*, 2017, **9**, 11082-11094.

27 Y. Li, Y. Su, X. Zhao, X. He, R. Zhang, J. Zhao, X. Fan and Z. Jiang, *ACS Appl. Mater. Interfaces*, 2014, **6**, 5548-5557.

28 X.-N. Chen, L.-S. Wan, Q.-Y. Wu, S.-H. Zhi and Z.-K. Xu, *J. Membr. Sci.*, 2013, **441**, 112-119.

29 K. Zhao, X. Zhang, J. Wei, J. Li, X. Zhou, D. Liu, Z. Liu and J. Li, *J. Membr. Sci.*, 2015, **492**, 536-546.

30 Y. Li, L. H. Wee, A. Volodin, J. A. Martens and I. F. Vankelecom, *Chem. Commun.*, 2015, **51**, 918-920.